4-2014

Comparing Methods for Full Body Inverse Dynamics Analysis of a Standing Long Jump

Nathaniel Vlietstra
Grand Valley State University

Comparing Methods for Full Body Inverse Dynamics Analysis of a Standing Long Jump

Nathaniel Vlietstra

A Thesis Submitted to the Graduate Faculty of

GRAND VALLEY STATE UNIVERSITY

In

Partial Fulfillment of the Requirements

For the Degree of

Masters of Science in Engineering

Padnos College of Engineering and Computing

April 2014

Acknowledgments

Special thanks are in order for my advisor Dr. Blake Ashby for all his support, experience and work throughout this entire project, and to my committee members Dr. Gordon Alderink and Dr. John Farris for their knowledge, reviews and advice on data collection and writing. I would also like to thank the staff of the Grand Valley State University statistical consulting center for their advice and expertise in summarizing my results.

Abstract

The classic iterative Newton-Euler method for inverse dynamics applied to calculating net joint torques in biomechanics analysis has a number of drawbacks. Many sources of error including imprecision in video motion capture data measurements can lead to significant errors in calculated net joint torques. Adding ground reaction force data overconstrains the solution. This study examined the effectiveness of various inverse dynamics analysis methods on a full body analysis of the standing long jump motion. These methods included variations in which equations for segments from the link-segment model were removed to relieve over constraint. Also considered were analysis methods applying least squares optimization, which included all the measured data weighted in a least squares sense to fit to an overconstrained system.

Motion capture data of 48 total standing long jump trials were collected and analyzed. Conventional iterative solutions with and without including measured ground reaction forces, and least squares optimized inverse dynamics solutions were derived and applied to the kinematic data in a 2-dimensional, seven-segment, linked segment model of the full body. Net joint torques were calculated at six joints for a 1.5 s period immediately prior to take-off of each standing long jump, and joint power and total work performed at each joint was calculated over the entirety of each jump. The optimized least squares solution was shown to be very similar to the conventional iterative solution using ground reaction forces and removing the equations of motion at the trunk segment. Net mean torques at the elbow and shoulder were highly variable.

Table of Contents

List of Figures

1 Introduction

The standing long jump is an athletic event that has been used as a measure of athletic performance through much of history, including in the ancient and modern Olympic Games up to 1912. It is one of the simpler examples of jumping as a fundamental human movement. Since jumping requires strength, power, and coordination of the entire body, it has been frequently studied to analyze and improve athletic mechanics and performance (Ashby & Heegaard, 2002; Payton & Bartlett, 2007). Jumping involves more extensive coordination of the upper and lower body movements, as compared to walking, which increases the complexity of analysis of jumping motions. Analysis of the biomechanics of the standing long jump is complex due to the extended motions, as well as the number of body segments contributing to the jumping motion and the number of muscles acting to various degrees on those segments (Hay, 1993).

A commonly used biomechanics analysis tool is inverse dynamics, a method which uses kinematic and kinetic data from a motion-capture system to calculate net torques at anatomical joints. These net torques can be used to infer (though not directly calculate) the muscle forces acting during the motion being studied. The conventional calculation of joint torques is completed by modeling the body as a series of rigid segments connected by joints and iteratively solving the Newton-Euler equations of motion for each segment in the model (Winter, 2009). While this solution is mathematically straightforward, noise in the measurement of segments' position, mass, centroid, and inertial moment lead to substantial errors. These errors propagate to the calculated linear and angular velocity and acceleration of each segment, compounding over and over as the solution to one segment is

used to solve for the next. Over the length of the model, which can include seven or more segments for the whole body, these errors can become larger than physiologically possible (Blajer, Dziewiecki, & Mazur, 2007; Hatze, 2002). Reaction forces at the ground can be measured by force plates and included in the equations of motion. However, introduction of reaction forces results in an overdetermined set of equations, so the equations for one segment must be arbitrarily ignored, or residual forces and torques applied, to calculate an explicit solution (Winter, 2009).

Previous work using the conventional approach removed the equations of motion for the trunk or forearm segment on the linked-segment model to eliminate the indeterminacy of the equations (Filush, 2012). However, removing the equations of motion for other segments from the model may yield more accurate net joint torques and is one consideration of this study. Alternative inverse dynamics approaches making use of all equations and all available data from ground reaction forces and motion capture have been applied to movement studies including gait analysis. These methods rely on static or dynamic optimization techniques (Andersen, Damsgaard, MacWilliams, & Rasmussen, 2010; Cahouët, Luc, & David, 2002; Chao & Rim, 1973), or least squares regression fits (Kuo, 1998; Van Den Bogert, Antonie J & Su, 2008). Application of these inverse dynamics techniques to biomechanics analysis of jumping activities is not evident in the scientific literature. Jumping motions have been analyzed with inverse dynamics, but only using the conventional approach to determine the contribution from upper body segments (Bisseling & Hof, 2006; Feltner, Fraschetti, & Crisp, 1999; Feltner, Bishop, & Perez, 2004; Filush, 2012; Pain & Challis, 2006; Vanezis & Lees, 2005).

The objective of the current study is to investigate various strategies for resolving the overdetermined system of equations in the inverse dynamics solution including:

1) Eliminating the three equations of motion for different segments to yield determinate conventional solutions,
2) Combining the different conventional solutions to spread the propagated error around the model, and
3) Simultaneously solving all of the equations using a least squares optimization solution method.

2 Background

A number of studies have examined various performance aspects of jumping biomechanics (Ashby & Heegaard, 2002; Ashby & Delp, 2006; Hatze, 1981; Hay, 1993; Wu, Wu, Lin, & Wang, 2003). Application of inverse dynamics methods to biomechanics is also well documented in the scientific literature (Andersen et al., 2010; Cahouët et al., 2002; Chao & Rim, 1973; Kuo, 1998; Van Den Bogert, Antonie J & Su, 2008). Application to jumping biomechanics is a smaller subset (Bisseling & Hof, 2006; Bobbert, Huijing, & van Ingen Schenau, 1987; Feltner et al., 1999; Feltner et al., 2004; Filush, 2012; Pain & Challis, 2006). The shortcomings of the conventional approach to musculoskeletal inverse dynamics are well described in literature (Winter, 2009), including compounding errors in iterative solutions and over determinate solution sets (Hatze, 2002). Several alternative methods of solving the inverse dynamics problem have been postulated (Blajer et al., 2007; H. R. Busby & Trujillo, 1987; H. Busby & Trujillo, 1997; Kuo, 1998; Van Den Bogert, Antonie J & Su, 2008) attempting to reduce errors and eliminate over-determinacies in the solution systems. These methods rely on least-squares fit solutions or similar cost optimization functions to improve the reliability of the analysis by using the over-determinacy caused by combining force plate and motion capture measurement.

2.1 Jumping Biomechanics Analysis

Calculated joint torque are used in biomechanics analysis to calculate the rate of power transfer through a joint, and also to infer which muscle groups are providing that power. In gait analysis, joint torque data are frequently used to diagnose musculoskeletal pathologies. In analyzing jumping, these data are used to evaluate the mechanisms relating

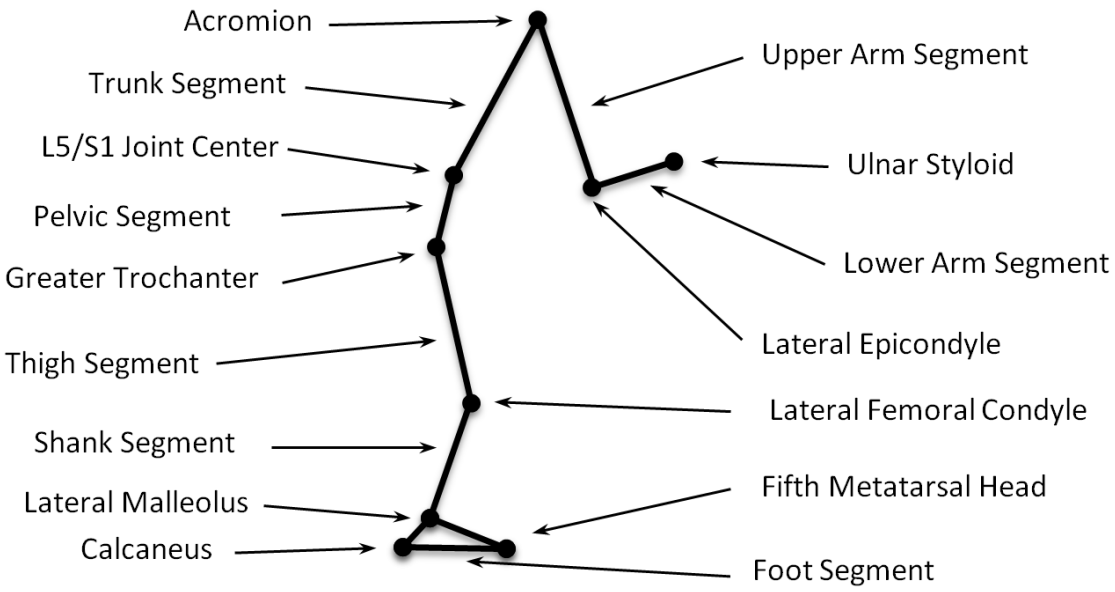

to improving jump distance. Inverse dynamics analysis can reveal fundamental motor control strategies that can be useful in optimizing sports performance or helping rehabilitate individuals with movement disabilities or deficits.

2.2 Conventional Inverse Dynamics Methods

The classic method of applying inverse dynamics to a 2-dimensional (or 3-dimensional) musculoskeletal system is relatively straightforward. A link-segment model of the body segments is constructed as shown in Figure 1 below. The head and trunk are modeled as a single continuous segment, as is the pelvic region including the spine below the L5/S1 vertebral joint. The forearm, wrist, and hand on each side of the body are all modeled as a single lower arm segment.

Figure 1: 2-dimensional projection of model segments and their relation to marker locations.

For the seven-segment model described in Figure 1, it is convenient to number the joints as follows:

1 – Ankle
2 – Knee
3 – Hip
4 – Lower back
5 – Shoulder
6 – Elbow

It is also appropriate to number the segments as follows:

1 – Foot
2 – Shank
3 – Thigh
4 – Pelvis
5 – Torso and head
6 – Upper arm
7 – Forearm and hands

The Newton-Euler equations of motion are applied progressively beginning at one end segment. This method is dependent on direction, starting at one end of the body and solving segment by segment using the results from the previous segment. Typically, the solution starts at the segment contacting the ground, and progresses up the model. A solution can also start at the hand(s) and solve each segment down, all the way to the ground if desired. This "top-down" solution assumes the reaction force and torque at the hand are zero. Air resistance is neglected for all the segments for all solution methods.

A generalized segment free-body diagram for segments 2 to 7 can be drawn with the segment angle in the first quadrant, as shown in Figure 2.

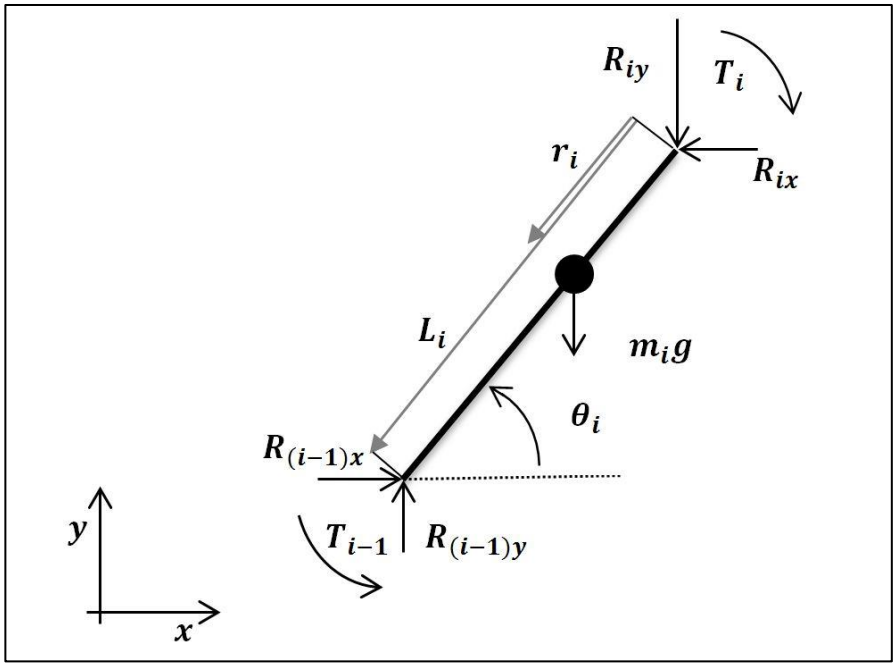

Figure 2: 2 dimensional free body diagram of a generalized segment.

For every segment, equations 2.1 to 2.3 are true:

$$\sum F_{ix} = m_i a_{ix} \tag{2.1}$$
$$\sum F_{iy} = m_i a_{iy} \tag{2.2}$$
$$\sum M_{iG} = I_i \alpha_i \tag{2.3}$$

Applying these equations to the free-body diagram in Figure 2 for $i = 2$ to 7 results in the following:

$$0 = -m_i a_{ix} + R_{(i-1)x} - R_{\mathrm{ix}} \tag{2.4}$$
$$0 = -m_i a_{iy} + R_{(i-1)y} - R_{\mathrm{iy}} - m_i g \tag{2.5}$$
$$0 = -I_i \alpha_i + T_{i-1} - T_i + R_{(i-1)x}(L_i - r_i)\sin\theta_i - R_{(i-1)y}(L_i - r_i)\cos\theta_i + R_{ix} r_i \sin\theta_i - R_{iy} r_i \cos\theta_i \tag{2.6}$$

The quantities in Equations 2.4 through 2.6 are:

$R_{(i-1)x}, R_{(i-1)y}$	Intersegmental force at the inferior joint in *x* and *y* directions, respectively
$R_{ix},\ R_{iy}$	Intersegmental force at the superior joint in *x* and *y* directions, respectively (equal to zero for segment 7)
T_{i-1}	Net joint torque at inferior joint
T_i	Net joint torque at superior joint (equal to zero for segment 7)
L_i	Segment length
r_i	Distance from superior joint to segment mass center
θ_i	Segment angle relative to x (horizontal) axis
m_i	Segmental mass
g	Gravitational constant
α_i	Segment angular acceleration
a_{ix}, a_{iy}	Segment mass center acceleration in *x* and *y* directions, respectively
I_i	Segment mass moment of inertia with respect to its mass center

The distal end of the foot segment is modeled as a moving contact with the ground. The foot segment does not have an applied moment at the ground, but does have a measurement of the center of pressure (COP) that locates where the reaction forces at the ground act on the foot. As the foot is treated differently than the rest of the modeled segments, an additional free-body diagram is shown in Figure 3.

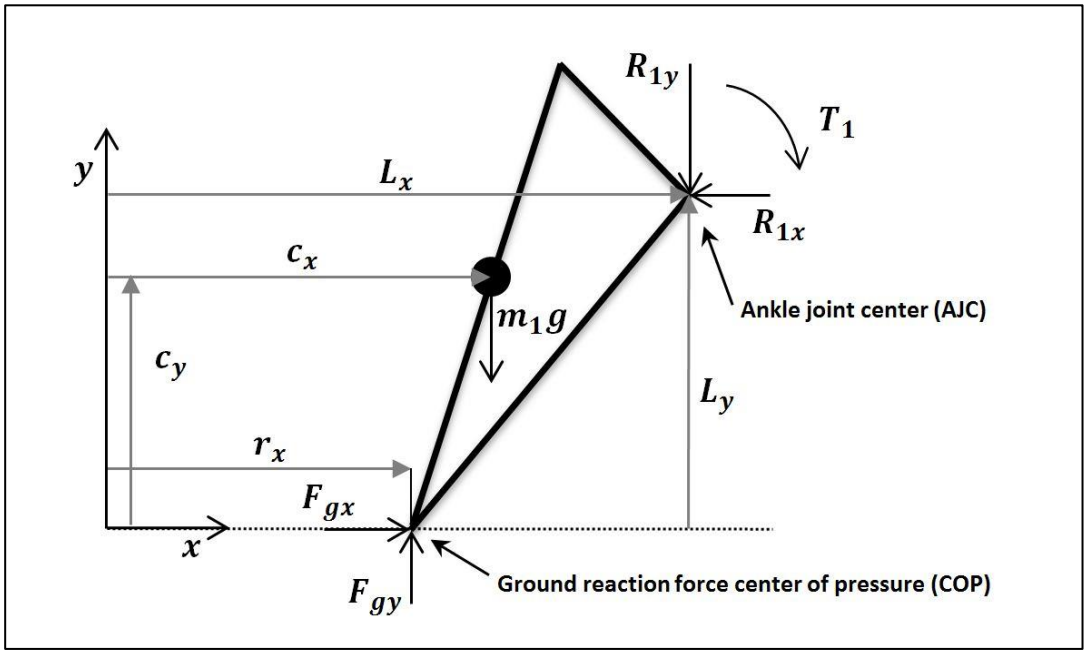

Figure 3: Free body diagram of foot segment at takeoff.

As with Equations 2.4 to 2.6 above, equations of motion 2.7 to 2.9 apply to the foot segment:

$$0 = -m_1 a_{1x} + F_{gx} - R_{1x} \quad (2.7)$$

$$0 = -m_1 a_{1y} + F_{gy} - R_{1y} - m_1 g \quad (2.8)$$

$$0 = -I_1 \alpha_1 - T_1 + F_{gx} c_y - F_{gy}(c_x - r_x) + R_{1x}(L_y - c_y) - R_{1y}(L_x - c_x) \quad (2.9)$$

The terms in Equations 2.7 to 2.9 are:

R_{1x}, R_{1y}	Intersegmental force at the ankle joint center in *x* and *y* directions, respectively.
F_{gx}, F_{gy}	Ground reaction force in *x* and *y* directions, respectively
T_1	Net joint torque at ankle
$L_x,\ L_y$	Distance from origin to ankle joint center in the *x* and *y* directions, respectively
r_x	Distance from origin to the COP in the *x*
$c_x,\ c_y$	Distance from origin to foot mass center in the *x* and *y* directions, respectively
m_1	Foot segment mass
g	Gravitational constant
α_1	Foot angular acceleration
a_{1x}, a_{1y}	Foot mass center acceleration in *x* and *y* directions, respectively
I_1	Foot mass moment of inertia with respect to its mass center

For this 2-dimensional link model with seven segments there are 21 equations of motion (Equations 2.1 to 2.3). Each of the six intersegmental joints introduces three unknowns (the *x* and *y* direction intersegmental forces and the net joint torque) resulting in 18 unknowns for the system. The loading conditions are assumed to be zero at the hands. The interaction between the feet and ground introduces three more unknowns (x and y direction ground reaction forces and the location of the center of pressure in the x direction). This results in a completely defined system with 21 equations and 21 unknowns. However, if the ground reaction forces are measured by force platforms at the feet and applied to the model, the system becomes overdefined with three more equations than unknowns.

Several separate (and independent) iterative inverse dynamics solutions to the link-segment model can be calculated by applying the known loading conditions at one or both ends of the model:

1) Using the measured ground reaction forces to include the force on the end of the foot, the "bottom-up" (bottom-up) explicit solution can be calculated. This solution is solved iteratively from the foot to the forearm, either disregarding the equations of motion for the forearm segment or calculating a residual force and torque at the hand, which is a known error (since no external forces and torques are applied at the hand).

2) Starting at the hand/forearm segment and assuming the forces and moments at the hand are zero results in a "top-down" (top-down) solution, solved iteratively from the forearm to the foot. This solution either disregards the equations of motion for the foot segment or calculates a residual ground reaction force result (which may not be the same as a measurement of the actual force at the ground).

3) Discarding the equations of motion for any one segment allows the "top-down" solution to the superior end of that segment, and the "bottom-up" to the inferior end. This is equivalent to obtaining both the bottom-up and top-down solutions and discarding results for all joints beyond the chosen segment, as discussed in Sections 5 and 6 below.

2.3 Conventional Inverse Dynamics Issues

The major drawback of inverse dynamics analysis using motion-capture data is the compilation of errors from all the measurements and calculations required to derive joint torque estimates. These errors arise from a variety of sources, including experimental and systemic errors, and are worth an exhaustive description.

First, the measurement of marker position data in real-time has associated errors from noise and calibration inaccuracies. When joint centers are approximated by marker locations a difference invariably exists between the modeled center of rotation and the anatomical joint center. The repeatability of marker placement on the body contributes to this issue. Even if the markers were able to be placed with perfect accuracy and exact repeatability and precisely tracked, the soft tissues of the limbs allow the marker to move relative to the bone. This causes artifacting when the segment and marker accelerate at different rates due to the compliance of the tissues connecting the two (Pain & Challis, 2006; Peters, Galna, Sangeux, Morris, & Baker, 2010). Error in the marker position data also compounds when numerically differentiating the discrete data points to obtain segment velocities and again when calculating accelerations.

Segment specific parameters including mass, mass moment of inertia, mass center location, and segment lengths cannot feasibly be measured directly. These values are estimated based on the height and weight of the participant, using tables of typical values (Plagenhoef, Evans, & Abdelnour, 1983; Winter, 2009). This estimation necessarily introduces some error in values which are used in further calculations. Finally, the link-segment model also assumes pure rotational joints, and in the 2-dimensional model all rotation is assumed to be in the sagittal plane. However, anatomical joints experience both rotation and translation about and along multiple axes during movement. The 2-dimensional projection of this rotation in the link-segment model introduces additional error to the calculated values due to the simpler model.

All of these errors compound when moving along the chain of segments, getting progressively worse at each step. Because each segment solution depends on the reaction

forces from the previous segment, any errors in the calculated values for one segment will propagate to the adjacent segments. Thus, the accuracy of forces and torques calculated on the first segment has a profound effect on the reliability of the calculated values further up the model. Since the forces and torques are calculated directly from the second derivative of position data from a video motion capture system, any noise in the position measurement increases non-linearly in the calculation of velocity, and again for acceleration (Hatze, 2002).

In the particular case of the segment in contact with the ground (typically the foot segment), the distal reaction force can be directly measured by a force sensor. The precision and resolution of the data recorded by the force plate are typically superior to those calculated from mass property estimation and derived accelerations. To more accurately measure the forces on the initial segment, force plate data can be used to provide known values for the reaction forces and moment for the segment end nearest the ground, which in this model are the distal ends of the foot segments. This results in one segment having well-defined input forces and moments, but eliminates three unknowns from the inverse dynamics solution and the solution becomes overconstrained (Hatze, 2002). This can be resolved by simply ignoring the set of equations for one segment, normally the set furthest removed from the initial segment (Winter, 2009). In cases where the reaction forces or applied loading of interest occurs on the segment furthest away from the initial segment, this resolution is not particularly satisfactory, since these loads do not show up at any point in the inverse dynamics calculation. In this case a set of equations for another segment can be removed (Filush, 2012).

The exact effect choosing to remove segments other than the one furthest from the ground has on the final calculated joint torque values is unclear. Winter (2009) implies that leaving out the top segment equations provides the most reliable results relative to forward simulations. However a direct comparison between analyses showing that effect is not present in the literature. Examining this question is one of the primary objectives of this study.

2.4 Inverse Dynamics: Optimization Methods

Kuo (1998) proposed an alternative method for inverse dynamics which solves all of the equations simultaneously in a least squares sense to find the joint torques that best satisfy the equations. In this study, the overconstrained inverse dynamics equations were represented by:

$$\boldsymbol{A} \cdot \boldsymbol{T} = \boldsymbol{b} \tag{2.10}$$

where $\boldsymbol{A}$ is the non-square matrix containing the coefficients of the joint torques in the equations of motion, $\boldsymbol{T}$ is the vector of joint torques, and $\boldsymbol{b}$ is the vector of known forces and torques.

Kuo evaluated the methodology for this alternative method on an overconstrained 2-dimensional system using the known results from a forward dynamic simulation. Prior to performing the inverse dynamics analysis, the $\boldsymbol{A}$ matrix was multiplied by a diagonal matrix $\boldsymbol{W}$ which effectively represented artificially added measurement "noise" to simulate experimental results:

$$\boldsymbol{W} \cdot \boldsymbol{A} \cdot \boldsymbol{T} = \boldsymbol{b} \tag{2.11}$$

The least squares solution for the joint torques $\boldsymbol{T}$ was calculated using the pseudo-inverse as follows:

$$\boldsymbol{T} = (\boldsymbol{A^T} \cdot \boldsymbol{W^{-1}} \cdot \boldsymbol{A})^{-1} \cdot \boldsymbol{A^T} \cdot \boldsymbol{W^{-1}} \cdot \boldsymbol{b} \quad (2.12)$$

Kuo demonstrated a 30% reduction in error in calculated joint torques compared to a conventional analysis, with both solutions being compared to a forward simulation. The forward simulation in this study was both the source of the data for analysis, and the known answer to which the processed data could be compared.

Van den Bogert et al. (2008) proposed an alternative method also using a least squares solution, which expanded on Kuo's work to a 3-dimensional system and analysis of partial ground reaction data (i.e. a partially instrumented treadmill). They compared the error between the conventional and alternative methods on measured data, and compared noise to estimated noise derived from a Monte Carlo simulation.

Van den Bogart generalized the least squares solution method to 3-dimensional analysis; however 3-dimensional inverse dynamics adds considerable complexity. Whether 3-dimensional analysis enhances the precision of inverse dynamics of jumping is not entirely clear in the literature, and is a potential area for further study. The scope of this study is limited to 2-dimensional analyses.

A potential drawback to least squares solution methods is that they are static optimizations. The equations of motions are solved at each point in time independent of the equations at the previous or following points in time. The solutions for the joint moments are therefore not entirely dynamically consistent over time and thus will not precisely reproduce the measured motion when applied to the model and integrated forward in time.

2.5 Comparing Inverse Dynamics Methods

As the loading conditions are measured or assumed known at both ends of the link segment model of the body, for a conventional inverse dynamics solution, the error in the solution typically increases for joints further from the known end loading. For example, the error in the ankle torque should be relatively small for the bottom-up solution and relatively large for the top-down solution. Conversely, the error in the elbow torque should be relatively small for the top-down solution and relatively large for the bottom-up solution. The least squares solution effectively spreads the errors throughout all the joint solutions. Therefore, the least squares optimization is expected to generate values in between the iterative top-down and bottom-up solutions. If this is the case, then the least squares solution may be comparable to a weighted mean of the two solutions.

3 Experimental Design

Standing long jump trials were conducted using a motion capture system consisting of eight cameras and two force plates (as described in Section 3.2) and a set of reflective markers (as described in Section 3.3). The reflective markers were placed on the body and allowed data to be collected for kinematic and kinetic analyses of both upper and lower body segment motion. Force plates were used to capture the ground reaction forces and locations of the center of pressure. The jumping trials and marker locations were also documented with video and still photography.

3.1 Participant Selection

Six young (range: 18-28 years) adult male volunteers [Mean ±StdDev: 90.3±12.0 kg, and 182.0±6.3 cm] were selected for experimental jumps. All participants completed a survey to determine a minimum of occasional physical fitness activity and any injury history which could increase the risks associated with jumping. Each volunteer participated in one session, approximately one hour in duration. The six sessions were performed over the course of several days. The participants were informed of the risks associated with the study and gave their consent to participate. The experiment protocol was reviewed and approved by the Human Research Review Committee at Grand Valley State University.

3.2 Experimental Procedure

Reflective markers were placed on every participant by the same researcher for consistency, and marker placement was verified by a physical therapist with 20 years of gait analysis experience. Participants were instructed to warm-up to increase jumping performance and reduce the risk of injury by jogging at a self-selected comfortable speed

for 5 minutes on a treadmill, and were allowed to stretch if desired. The participants were given the opportunity to execute practice jumps to reduce the internal variability between each participant's trials by allowing each to establish a personal routine for the jump.

For each participant, separate static standing trials were collected on two force plates to determine each participant's mass, and to observe the complete marker set for joint center calculations. Jumping trials immediately followed the standing trials. The participants were instructed to perform standing long jumps for best distance, jumping from both force plates simultaneously with one foot on each plate during takeoff. The participants performed eight jumps sequentially at approximately one-minute intervals.

3.3 Equipment and Data Collection

Segment position data were captured using a Vicon motion capture system (Vicon Motion Systems Ltd., Los Angeles, CA) consisting of eight cameras that record the three dimensional locations of reflective markers placed on the body. Each camera recorded the locations of the reflective markers in its field of view at 120 Hz, using infrared LED strobes. As the participants moved through the motion capture field of view, the strobes reflected off the markers attached to the body allowing each camera to return the markers' 2 dimensional projections onto the camera's field of view. The Vicon data station recorded the position data from the cameras, and then passed the information to the Nexus software where markers were isolated and labeled, and post-processed to determine the 3D positions of the markers. The Vicon camera system was calibrated prior to each session.

To capture ground reaction forces and center of pressure locations the participants were instructed to jump off a pair of an in-ground AMTI force plates (Advanced Mechanical Technology Inc., Watertown, MA). The total force on both plates was summed

to determine the total ground reaction forces up until the point of takeoff. The average of the center of pressure (COP) location measured by each force plate was taken to determine the overall COP location in the x (jumping) direction, while the y (vertical) direction COP was set to zero throughout the propulsive phase of each jump.

3.4 3 Dimensional Marker Locations and Segment Definitions

The marker locations chosen allowed a model to be constructed, and then simplified in a projection of the left half of the body in the sagittal plane. The reflective markers were placed on the skin, and on top of clothing or shoes, in locations intended to allow sufficient data to be collected to perform kinematic and kinetic analyses of the upper and lower body segments of a three-dimensional link-segment model. The marker locations relevant to the 3D model and its 2D projection included: the fifth and first metatarsal heads (toe), the lateral and medial malleoli (ankle), the lateral and medial femoral condyle and fibular head (knee), the greater trochanter (hip), the acromion (shoulder), the lateral and medial epicondyles of the humerus (elbow), and the ulnar and radial styloids (wrist). Additional markers were placed specifically on the thigh, shank, trunk, upper arm, forearm, and hand segments, and are visible in Figure 4.

These markers fully define reference coordinate systems for a 3-dimensional, 12-segment model of the entire body. These data are useful for additional research outside the scope of this study, but were not used in the sagittal plane projection to the 2D model under consideration here.

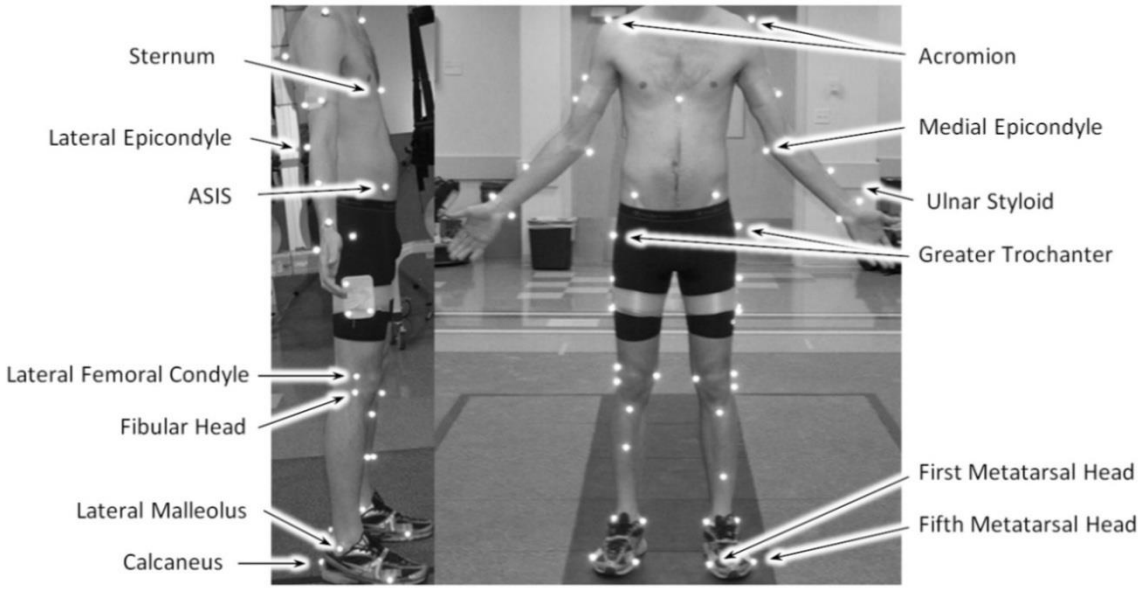

Figure 4: Sagittal (l) and Frontal (r) plane marker locations.

For segment length calculation purposes, the calcaneus, greater trochanter, and acromion markers were taken to approximate the proximal end of the foot, the hip joint center, and the shoulder joint center, respectively. The L5/S1 vertebral joint center was taken as the center of rotation at the lower back, and its location was calculated based on the posterior and anterior superior iliac spines (PSIS and ASIS) marker position using the formula described by Lariviere et al. (2001), and the pelvic inertial properties described by McConville et al. (1980) and Plagenhoef et al. (1983). Segment mass, center of mass, and inertial properties were used as defined by Winter (2009). The segment parameters used for each participant are listed in Appendix A.

Segment lengths were calculated from data collected during static (non-jumping) anatomic position standing trial, once per participant on each force plate. Segment lengths were defined by distances between joint centers at the toe, ankle, back, elbow, and wrist, as follows:

Foot: Center of 5^{th} and 1^{st} metatarsal markers to calcaneus marker
Shank: Center of malleoli markers to center of femoral condyle markers
Thigh: Center of femoral condyle markers to the greater trochanter
Pelvis: Greater trochanter to L5/S1 joint center.
Trunk: L5/S1 joint center to acromion marker
Upper Arm: Acromion marker to center of humeral epicondyle markers
Lower Arm: Center of epicondyle markers to center of styloid markers

To ensure that markers used to calculate joint centers and segment lengths were visible to the camera system, segment lengths were calculated from static trials in the anatomical position with the foot, shank, thigh, pelvis and trunk projected into the sagittal plane. The upper and lower arms segment lengths were projected into the frontal plane since they deviate significantly out of the sagittal plane when measured in the anatomical position. All segment lengths were assumed to be constant throughout the whole duration of a participant's jumps, and were not dynamically calculated during the jump.

3.5 Simplification to a Sagittal Plane Model

Bilateral symmetry was assumed for marker locations, and the left half of the body was used for the 2D simplification. The marker locations selected allow for projection onto the sagittal plane such that the endpoints of 2D model segments correspond to marker locations, as shown in Figure 1. As some medial markers were hidden from view during the jumps, the lateral markers at the ankle, knee, elbow, and wrist (as shown in Figure 4) were used to calculate segment angles. Segment angles for a segment with endpoints at positions $(x_{i-1}, y_{i-1}), (x_i, y_i)$ were calculated by Equation 3.1:

$$\theta_i = \operatorname{atan}\left(\frac{y_i - y_{i-1}}{x_i - x_{i-1}}\right) \tag{3.1}$$

4 Data Analysis

Nexus 1.8.4 (Vicon Motion Systems Ltd., Los Angeles, CA) software was used to capture and compile the raw kinematic and force results of the jumping trials for analysis. The data were analyzed using Wolfram Mathematica 9.0 (Wolfram Research, Inc., Champaign, IL) and MatLab R2013a (Mathworks, Natick, MA) software. The analysis consisted of data filtering, application of conventional inverse dynamics and least squares solutions, and comparing the solution output.

The raw data captured by the Vicon system was processed in Nexus to apply the model. Ghost marker artifacts were removed and small gaps in the marker data were filled with spline interpolations. The raw data were filtered to remove high frequency noise and isolate the data relevant to segment motion. Physiological factors limit relevant anatomical motion signal to approximately 3-5 Hz at the trunk and 5-10 Hz at the extremities, with frequencies above 10 Hz almost entirely noise while jumping (Wells & Winter, 1980). A bidirectional low pass Butterworth filter with a cutoff frequency of 10 Hz was used to filter both the motion capture data and the ground reaction force data in Math Works MatLab R2013.

The ground reaction force data was subsampled at a 1:10 ratio to correspond to the 120 Hz framerate of the motion capture data, and the time where the reaction forces went to zero defined as takeoff. Data were clipped at takeoff and 1.5 s (181 frames) before takeoff for analysis. The 1.5 s period was sufficient to capture the standing and propulsion phases of the jump up to takeoff for all 48 trials, except for one trial where the system failed to capture the first 24 frames (0.18 s) of the 1.5 s period.

4.1 Conventional Inverse Dynamics

The equations of motion were derived in full for all seven segments (21 equations, see Appendix B for the full list of equations). Conventional inverse dynamics using iterative solving of the Newton-Euler equations of motion for each segment were performed completely from the hand to the ground (top-down) and the foot to the hand (bottom-up). Solutions ignoring particular segments were not individually calculated as such solutions are identical to comparing the top-down and bottom-up solutions across particular segments.

Kinematic analysis was performed in Wolfram Mathematica using forward differences to twice numerically differentiate segmental center of mass positions and angles. The resulting segmental angular and center of mass accelerations were applied to the equations of motion using mass and inertial properties as described in section 3.4 above, to calculate net joint torques at every time frame over the 1.5 s before takeoff.

The net torque at each joint was calculated using both top-down $(T_{TD,i})$ and bottom-up $(T_{BU,i})$ solutions and also combined into the proposed weighted mean $(T_{WM,i})$ conventional solution. This is the mean of the top-down and bottom-up solutions, weighted linearly by the number of segments separating each solution from the nearest known applied force (at either the hands or the feet). For joint *i* from 1 (ankle) to 6 (elbow), the weighted mean net joint torque is:

$$T_{WM,i} = \frac{i-1}{5} T_{TD,i} + \frac{6-i}{5} T_{BU,i} \tag{4.1}$$

4.2 Alternative Inverse Dynamics

A least squares fit inverse dynamics analysis was performed on the jumping trial data. The joint torques and intersegmental reaction force vector acting on each segment calculated through this analysis were compared to the conventional analyses. While a comparison to the "real answer" cannot be made since net joint torques cannot be physically measured, the solution is readily compared to other solutions.

Equations 2.4 through 2.9 can be specified for all joints and combined in matrix equation form to obtain a least squares optimized solution. This is done by defining the matrices $\boldsymbol{x}$, $\boldsymbol{A}$, and $\boldsymbol{b}$, where $\boldsymbol{x}$ is the vector of intersegmental force and joint torque quanties defined for every *joint* using Equations 2.4 through 2.9:

$$\boldsymbol{x} = \begin{bmatrix} R_{1x} \\ R_{1y} \\ T_1 \\ \vdots \\ R_{6x} \\ R_{6y} \\ T_6 \end{bmatrix} \tag{4.2}$$

Next, $\boldsymbol{b}$ is the vector of constant mass and inertial properties, and measured accelerations for every segment, and $\boldsymbol{A}$ is the matrix of all coefficients for the equations including every segment and joint. See Appendix C for a full description of $\boldsymbol{A}$ and $\boldsymbol{b}$. Equations 2.1 through 2.3 then simplify to:

$$\begin{bmatrix} 0 \\ \vdots \\ 0 \end{bmatrix} = \begin{bmatrix} \sum F_{x1} - m_1 a_{1x} \\ \sum F_{y1} - m_1 a_{1y} \\ \sum M_{G1} - I_1 \alpha_1 \\ \vdots \\ \sum F_{x7} - m_7 a_{7x} \\ \sum F_{y7} - m_7 a_{7y} \\ \sum M_{G7} - I_7 \alpha_7 \end{bmatrix} = \boldsymbol{A} \cdot \boldsymbol{x} - \boldsymbol{b} \tag{4.3}$$

The coefficients matrix $\boldsymbol{A}$ and the constants matrix $\boldsymbol{b}$ are calculated using the known values for segment angle, mass, inertia, and length (a sample implementation of the calculation is shown in Appendix B). Equation 4.3 has no exact solution since $\boldsymbol{A}$ is longer than $\boldsymbol{x}$, but the least squares solution can be found by the static optimization shown in equation 4.4.

$$\boldsymbol{x} = argmin_x[|\boldsymbol{A} \cdot \boldsymbol{x} - \boldsymbol{b}|^2] = (\boldsymbol{A^T} \cdot \boldsymbol{A})^{-1} \cdot \boldsymbol{A^T} \cdot \boldsymbol{b} \tag{4.4}$$

Both conventional and least squared solutions were applied for every video capture frame to calculate joint torques 120 times per second over the entire 1.5 s period before takeoff.

4.3 Net Joint Power and Work

The joint power P_i at each joint i was calculated as:

$$P_i = T_i(\omega_i - \omega_{i+1}) \tag{4.5}$$

In equation 4.5, ω_{i+1} is the angular velocity of the superior segment, while ω_i is that of the inferior segment and T_i is the net torque at joint i.

The net joint work W at each joint i was integrated as joint power over time:

$$W_i = \int_{-1.5\ s}^{0} P_i dt \tag{4.6}$$

Power and work were calculated using the net joint torques from each of the four solution methods, at every joint.

4.4 Comparing Methods

Statistical models were created in SAS JMP 10.0 (SAS Institute, Cary, NC, USA) to compare the joint work and torques calculated by each various inverse dynamics method. A one-way single variable ANOVA blocking on the six participants was used to calculate the mean joint torque at each frame, with 95% confidence intervals (See Table 5.2). Since 24 frames of data for one jump were not captured for one jump, N = 47 for those frames, with correspondingly wider confidence intervals than the rest of the jump sequence. For the last 157 frames, N = 48.

5 Results

The least squares (least squares) solution is compared to the bottom-up and top-down solutions in Figure 5 below. In Figure 6, the least squares solution is compared to the weighted mean of the two conventional solutions. In all plots, torque extending (or plantarflexing) a joint is represented as positive by convention. A one-way ANOVA statistical model was applied to the joint torques at each time frame to assess the differences the mean values and 95% confidence intervals as shown in Figure 5 and Figure 6, with the least squares solution compared to each conventional solution.

Net torque at each of the six joints was small and relatively constant during the initial phase of the jump, from about 1.5 s to 1 s before takeoff.

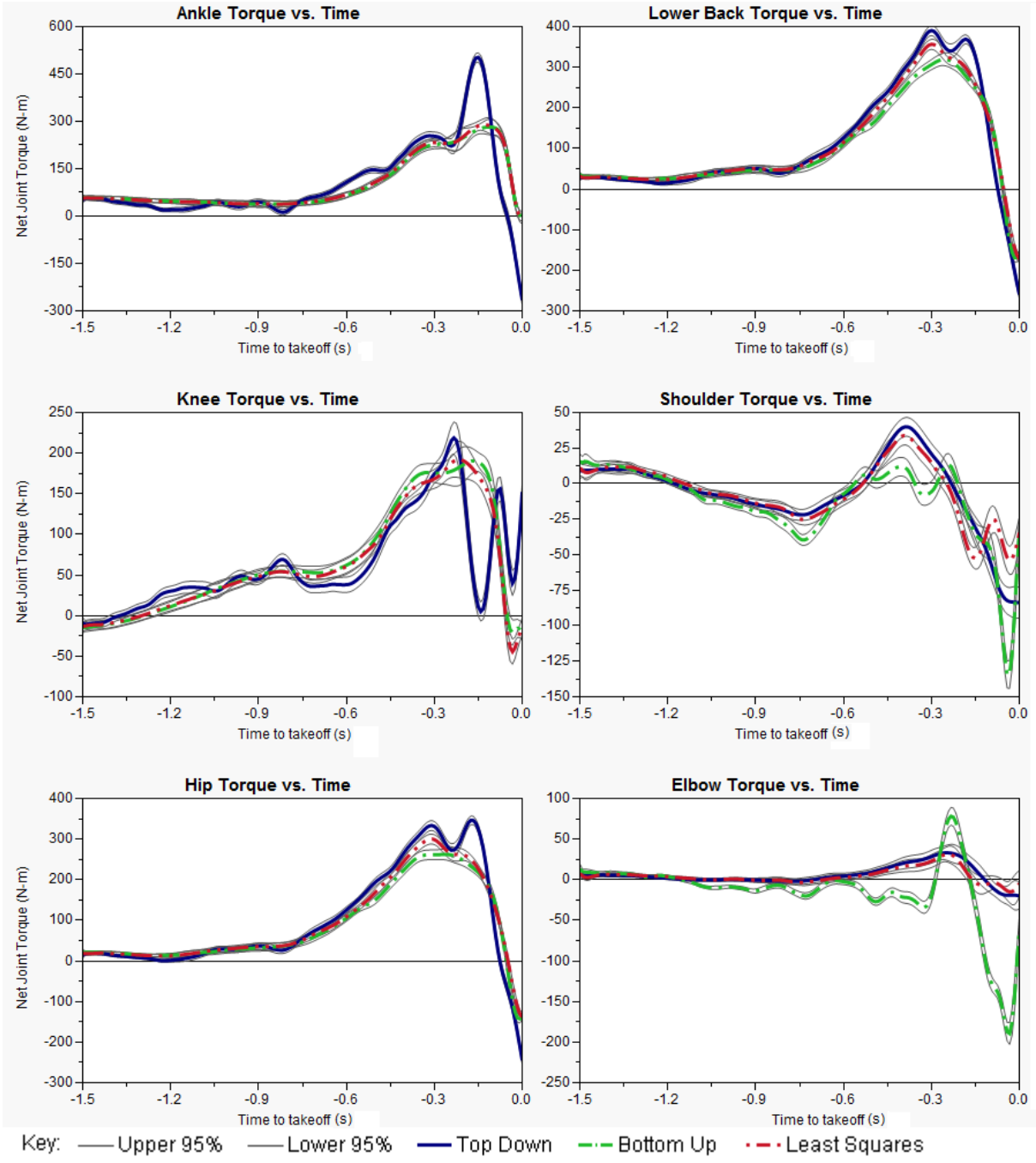

Figure 5: Joint torques for two conventional solutions and least squares solution.

Each joint experienced a peak extension torque during the propulsion phase of the jump, approximately 0.3 to 0.1 s before takeoff. The torque at each joint reversed to the

flexion direction during the 0.1 s immediately before takeoff, as the extending angular velocities were slowing to prevent joint hyperextension.

The three methods in Figure 5 are in the most agreement in calculating the hip and lower back torques, with overlapping confidence intervals through the jump at those joints. The least squares solution almost entirely coincides with the bottom-up solution at the ankle and with the top-down solution at the elbow.

The two joints furthest from the known force applied to the system (shoulder and elbow for bottom-up solution, knee and ankle for top-down solution) show substantial disagreement from the least squares solution in calculated mean torque over most of the jump. The 95% confidence intervals in all four cases do not entirely overlap for joints where solution is more than four segments from its respective starting point, suggesting that propagation of error across four or more segments is considerable.

The bottom-up and weighted mean methods are not substantially different from the least squares when calculating knee and ankle torque, and the top-down solution is reasonably similar for the first portion of the jump despite the number of segments separating it from the known force at the hand. The confidence intervals for all solutions also overlap for the initial phase of the jump. However, as the magnitude of the ankle and knee torques increase nearing takeoff, the difference between the top-down and bottom-up solutions increases considerably. For the propulsive phase, the top-down solution crosses out of the confidence intervals of the bottom-up and least squares solutions at the knee and ankle, indicating that there the difference increases as the velocity of the segments increases and the relative magnitude of the torques decreases.

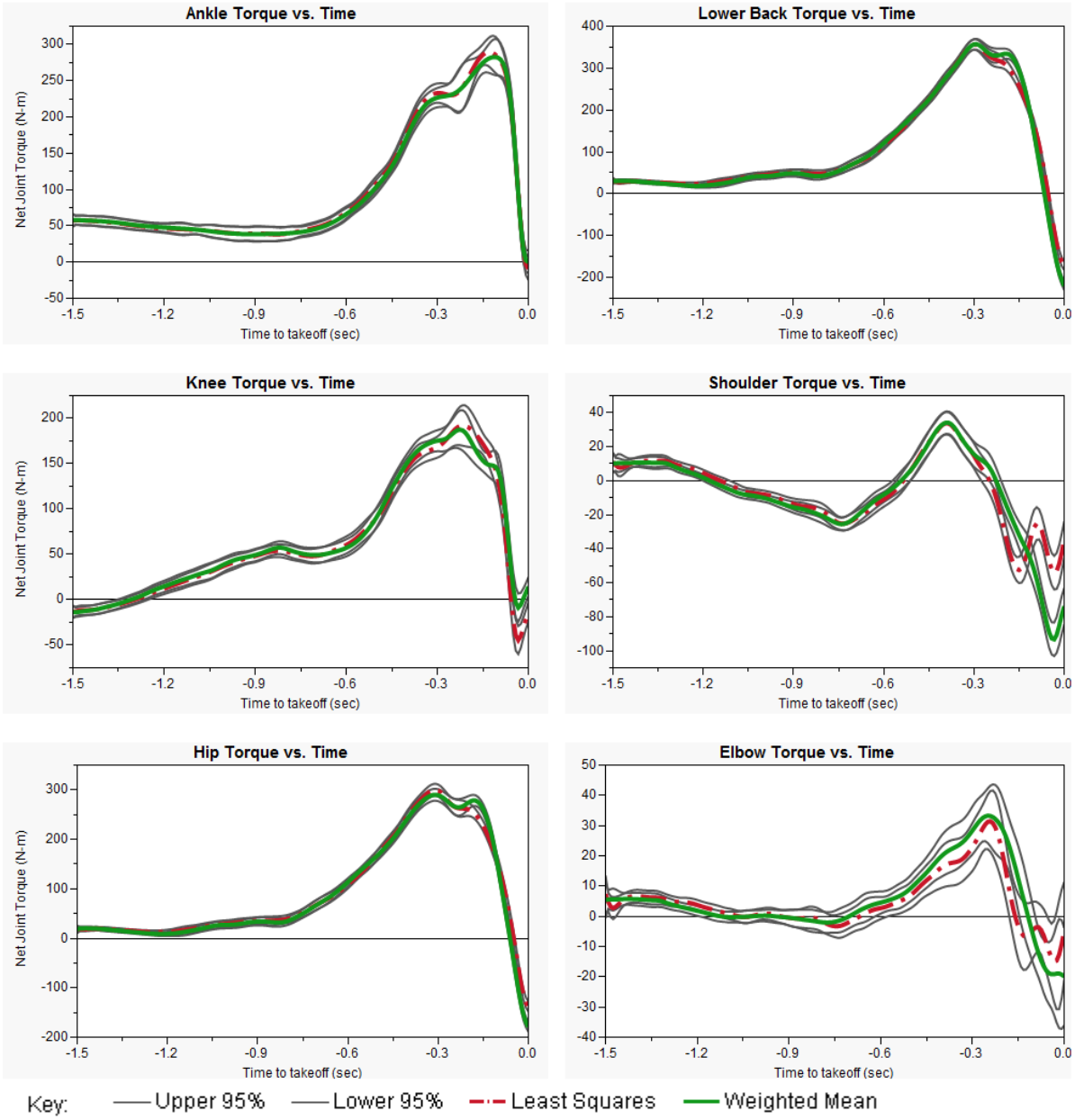

Figure 6: Mean joint torques for weighted means of conventional solutions vs least squares solutions.

The confidence interval of the weighted mean solution overlaps that of the least squares in the plots in Figure 6, for the four lower joints indicating that the weighted mean solution is not very different than the least squares analysis in the lower body. There is a difference between the weighted mean and least squares methods at the shoulder and elbow joints at the end of the propulsive phase of the jump. As in Figure 5, the torque at the elbow and shoulder is small relative to the variability and noise, especially as the segment velocity increases towards the end of the jump.

Joint power over time shown in Figure 7 is shown to correlate with joint torque as shown in Figure 5. The top-down solution matches the least-squares within the 95% confidence interval at the elbow, shoulder, back and hip. At the knee and ankle, the top-down solution deviates substantially from the least-squares solution during the propulsion phase. The reverse is evident with the bottom-up solution; at the elbow and shoulder it differs from the least squares solution while at the ankle, knee, hip, and back, the two solutions overlap.

The two joints above the trunk segment show good agreement between the top-down and least squares methods, and disagreement between the bottom-up and least squares methods in calculated joint power. Conversely, the four joints below the trunk show good agreement between the bottom-up and least squares method and disagreement between the top-down and least squares method calculated joint power.

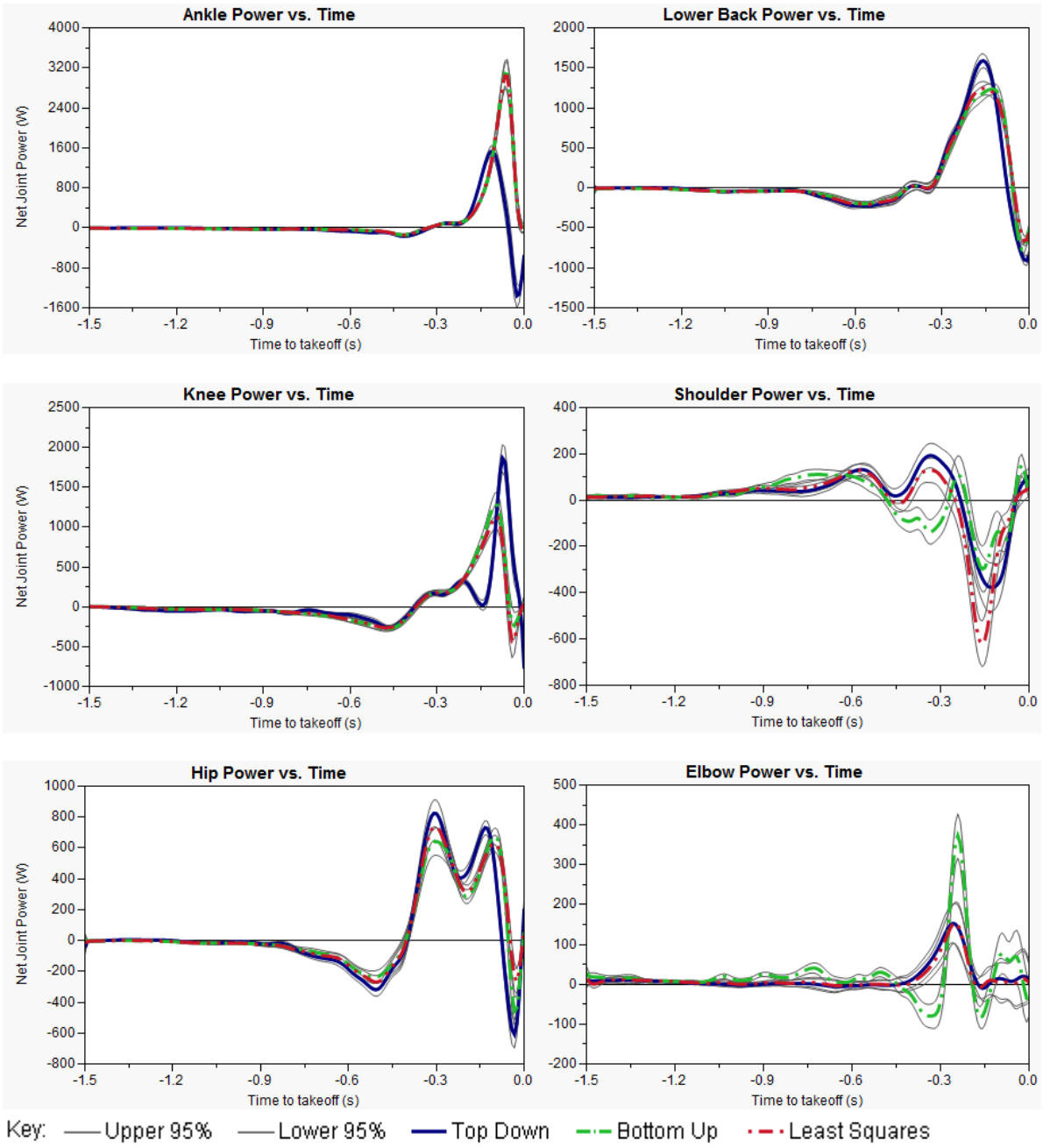

Figure 7: Mean joint power vs. time for two conventional solutions and least squares solution.

Joint powers calculated by the least squares and weighted mean solutions coincide nearly exactly as shown in Figure 8. While the mean values at the elbow joint are similar,

the 95% confidence intervals are much wider during the propulsive phase, where the segment center of mass velocity and angular velocity reach their maximums.

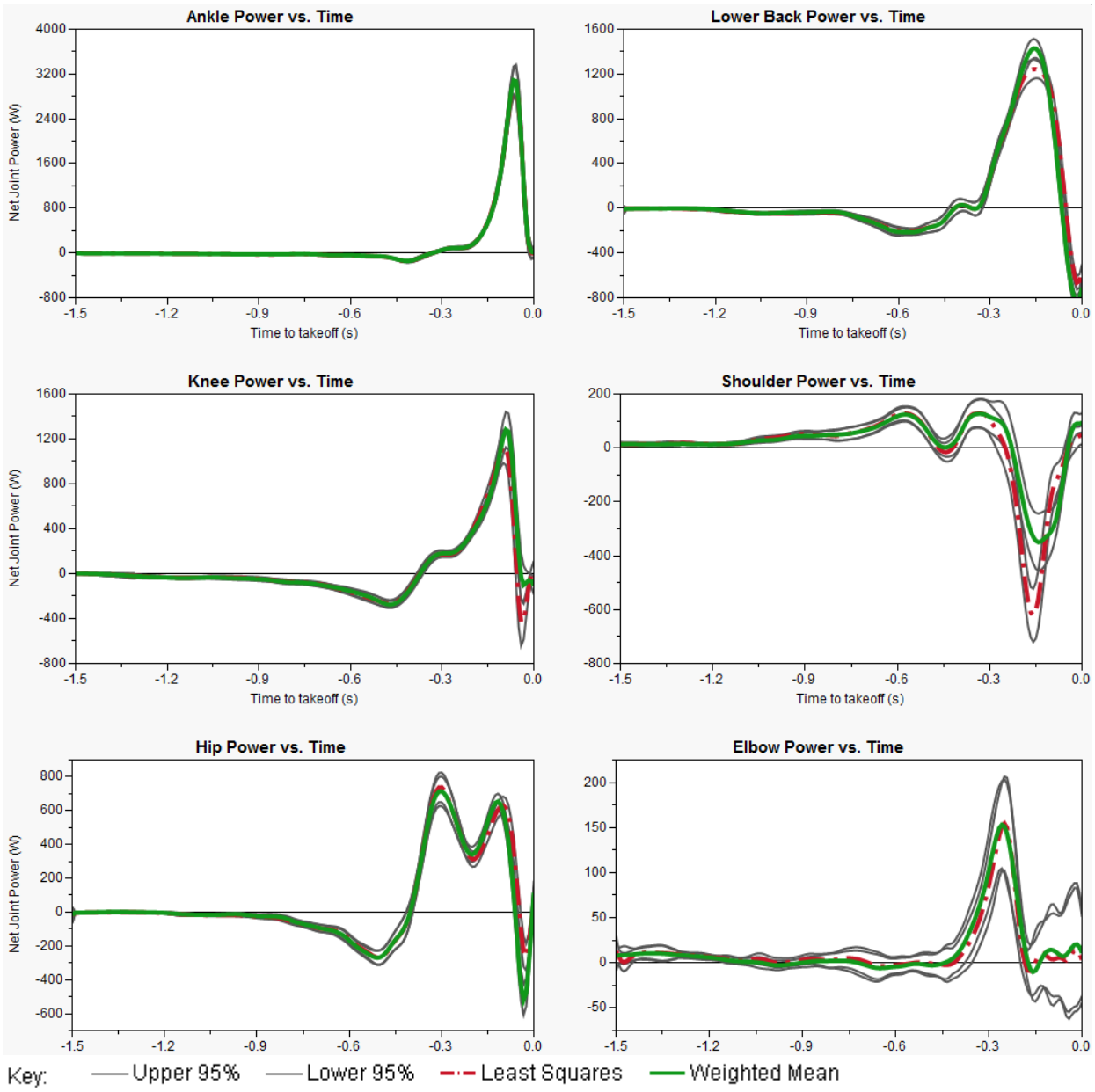

Figure 8: Mean joint power over time for weighted means of conventional solutions, and for least squares solutions.

Overall, the calculated net joint powers do not appear to be particularly different between the weighted mean and least squares solutions.

A one-way ANOVA was performed to determine the significance of variation in the mean joint work calculated by each method, and p-values for the mean difference ANOVA tests are given in Table 5.1. Differences that are significant ($p > 0.05$) are bolded.

Table 5.1: Statistical significance of differences in mean joint work calculated by various inverse dynamics methods

		Solution method pair:			
		least squares vs. bottom-up	least squares vs. top-down	least squares vs. weighted mean	top-down vs. bottom-up
Joint:	Ankle	0.9089	**<0.0001**	**0.0076**	**<0.0001**
	Knee	0.1093	0.3436	0.1393	0.9739
	Hip	0.1105	**0.0177**	**0.0430**	0.3810
	Back	0.5551	0.0808	0.2006	0.3212
	Shoulder	0.4922	**0.0007**	**0.0013**	0.4675
	Elbow	0.2086	0.6996	0.6996	0.2504

Net joint work was compared by method at each joint, and plotted in Figure 9 below. The mean net joint work calculated for each method was positive at every joint, consistent with the expectation that an efficient jump will create positive work at most or all joints.

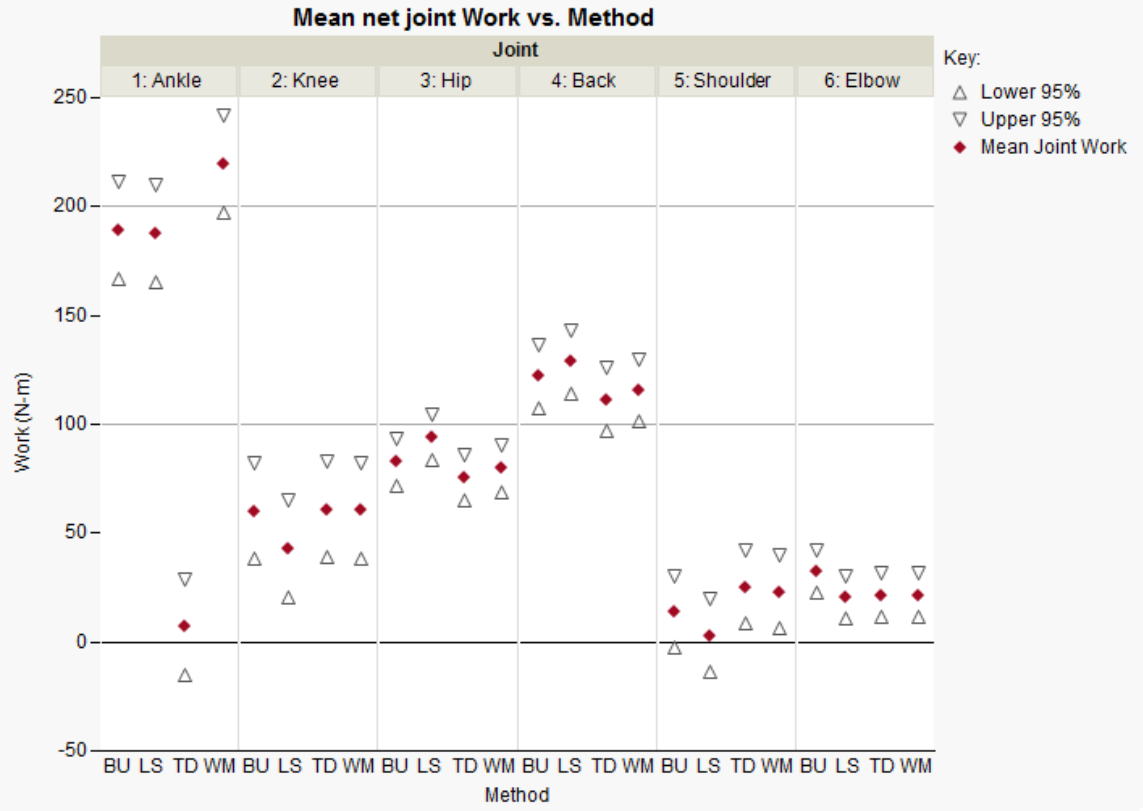

Figure 9: Mean net joint work for all solutions, with 95% confidence bounds.

The net joint work values calculated by each method are very similar, with the singular exception of the top-down calculated work at the ankle. All the remaining calculated values fall within or very near the 95% confidence interval for all other methods at the same joint. Statistical analysis to test the differences between the mean values showed little difference between methods.

Based on the calculated total joint work, the top-down solution is significantly different from all others at the ankle ($p<0.0001$). The bottom-up solution is not significantly different from the least squares method at any joint.

6 Discussion

Several of the results highlighted in Section 5 are consistent with the expected results of the analysis. Both Kuo (1998) and Van Den Bogert et. al (2008) showed that a least squares optimization produces similar calculated joint torques to a conventional solution, with some reduction in measured error, and the general similarities between the least squares, BD, and top-down solutions in Figure 5 are consistent with their work. Compared with the least squares solution, the large deviations of the bottom-up solution at the shoulder and elbow, as well as the large deviations of the top-down solution at the knee and ankle are consistent with the propagation of error through several segments of the model as discussed in Section 2.3. These dissimilarities in the solutions are visualized in Figure 5 and Figure 6, and in the case of the upper extremities are significant over the entire 1.5 s recorded duration of the jump. At the lower extremities the differences in the solution are only evident immediately prior to takeoff.

Examining the effects of discarding equations for various model segments does not require explicit separate analyses with one segment discarded in each solution. Instead, segments can be effectively discarded by comparing solutions up to the ends of the given segment. The agreement between methods changes the most when comparing the back and shoulder joints. These joints are at opposite ends of the trunk segment, suggesting that the trunk segment is the least consistent with the assumptions involved in a link-segment model. The trunk is not rigid or homogenous, but varies in density, length, and shape across time and between individuals. These results suggest avoiding calculation of inverse dynamics across the trunk segment from a known force input. For example, finding the net shoulder torque using a bottom up method with measured ground reaction forces is likely

much less accurate than assuming zero reaction force at the hand and using a top down method. Ignoring the equations of motion for the trunk segment yields joint torques of the full-body model that are most similar to a least-squares analysis, and calculates total work values which are not significantly different from a least squares optimization at any joint.

As the bottom-up method calculates substantially different torques at the shoulder than both the least squares and top-down solutions, discarding the upper arm equations does not appear to be a viable option – this will lead to substantial error at the shoulder. Discarding the pelvic segment equations, conversely, is appropriate, particularly in the five-segment model which is common in full-body 2D studies (Ashby & Heegaard, 2002; Filush, 2012; Hay, 1993; Wu et al., 2003). In this case, the trunk equations are also ignored and the shoulder and elbow torques are calculated from the top down.

Based on the calculated joint torques, all methods are somewhat different when calculating elbow torque, despite the elbow's proximity to the known force and torque at the hands (which are assumed to be zero). All methods differ visibly over time for some phases of the jumping motion, although the top-down and least squares substantially overlap in 95% confidence intervals, and are very similar to each other as opposed to the large variations in the bottom-up solution. The differences between all methods at the elbow are consistent with previous findings (Kuo, 1998) that segments with higher velocities have greater noise in derived accelerations, which propagates to variability in calculated torque. The results are also consistent with the observation that the 2D link-segment model assumptions of pure sagittal plane motion and bilateral symmetry are less valid for the upper extremities, causing relatively more error at the shoulder and elbow.

Based on calculated total joint work, the top-down solution is significantly different from all others at the ankle ($p<0.0001$), agreeing with the calculated joint torques results that the error propagation over more than four segments is relevant. At all joints except the ankle, the least squares, top-down, and bottom-up work values are not significantly different, suggesting that the total joint work calculation is not as sensitive as joint torque calculations to measurement noise. This is perhaps surprising considering that calculating the joint work requires the joint torque as an input, although it may simply be due to the noise increasing the confidence intervals and reducing statistical significance.

There is a significant difference in the work values calculated with the weighted mean and least squares methods at the upper extremity joints of the model. The differences at those two joints are most likely because error propagates (and increases) non-linearly through the system as the analysis moves away from the known starting point, and because the upper and lower arms are subjected to higher velocities and accelerations throughout the jump. The net torque is low and the changes in position over time (and the resulting errors) are large. Also, the assumptions of sagittal plane motion and bilateral symmetry again are less accurate at the upper extremities, and are likely contributing to the increased variability at the shoulder and elbow. Unlike the linearly weighted mean, the least squares solution method corrects to the error non-linearly. A more aggressive weighting profile may be more appropriate if the error propagation can be shown to increase at a non-linear rate. Such a model may be an area to be explored by future study. At the lower four joints, there is no noticeable difference between the weighted mean and least squares methods, and a weighted mean type of solution (particularly if further optimized) may be a simple

method to include the advantages of alternative inverse dynamics methods in future biomechanics studies.

7 Conclusion

Calculating net joint torques is a useful biomechanics analysis tool, but has no exact analytical or experimental solution. Application of the conventional methods for inverse dynamics to finding joint torques has a number of sources of error (including imprecision in video motion capture data measurements) which lead to significant noise and error in calculated net joint torques. Measuring ground reaction force data allows reduction of error if overdeterminacies in the resulting dynamics solutions can be resolved.

To compare inverse dynamics analysis methods, motion capture data of standing long jump trials were collected and ground reaction forces measured with force plates. Conventional iterative solutions and least squares optimized inverse dynamics solutions were derived and applied to the motion capture and force plate data in a 2-dimensional, seven-segment, linked segment model of the full body. Net joint torques were calculated at the six joints for a 1.5 s period immediately prior to take-off of each standing long jump, and joint power and total work performed at each joint was calculated over the entirety of each jump.

This study found that variability in calculated joint torque, power, and work values were shown to increase as segment equations were solved, iterating away from a measured reaction force. Segments with high linear and angular velocities, and segments moving or projecting out of the sagittal plane also showed increased variability.

In a full body analysis of the standing long jump motion, overdeterminacies can be resolved by removing equations of motion for the trunk segments of the link-segment model. This resolution has no substantial difference from a least squares optimized solution on the net torque, joint power, and joint work throughout the full body model. Linearly weighting the effect of all the segment's equations is also presented as a viable solution. Such conventional

analyses are shown to be highly consistent with analysis solutions applying least squares static optimization.

8 Appendices

8.1 Appendix A: Segment Parameters

Inertial parameters applied to segments:

Segment:	Mass:	Radius of Gyration:	Radius:
Foot	0.029	0.475	0.500
Shank	0.093	0.302	0.433
Thigh	0.200	0.323	0.433
Pelvis	0.142	0.500	0.895*
Trunk	0.436	0.503	0.340
Upper Arm	0.056	0.322	0.564
Lower Arm	0.044	0.468	0.318

Segment radius is the distance from the upper segment endpoint to the segment COM

Segments mass is relative to subject mass and radius is relative to segment length.

*Pelvic radius is relative to the distance from the acromion to the greater trochanter.

Appendix A, cont.

Segment properties, by Participant							
1	**Foot**	**Shank**	**Thigh**	**Pelvis**	**Trunk**	**UpArm**	**LwrArm**
Length (m)	0.22065	0.42920	0.43351	0.14057	0.46326	0.35797	0.28002
Mass (kg)	2.13651	6.85156	14.73453	10.46152	32.12127	4.12567	3.24160
Inertia (kg m^2)	0.02347	0.11511	0.28889	0.05168	1.72338	0.05481	0.05567
CG dist. (m)	0.11033	0.18584	0.18771	0.06338	0.15751	0.20189	0.08905
2	**Foot**	**Shank**	**Thigh**	**Pelvis**	**Trunk**	**UpArm**	**LwrArm**
Length (m)	0.22687	0.41076	0.39093	0.13405	0.48715	0.35746	0.24884
Mass (kg)	3.21113	10.29778	22.14576	15.72349	48.27775	6.20081	4.87207
Inertia (kg m^2)	0.03729	0.15846	0.35310	0.07064	2.86426	0.08215	0.06608
CG dist. (m)	0.11344	0.17786	0.16927	0.05612	0.16563	0.20161	0.07913
3	**Foot**	**Shank**	**Thigh**	**Pelvis**	**Trunk**	**UpArm**	**LwrArm**
Length (m)	0.18343	0.36523	0.40764	0.12886	0.47168	0.33274	0.22870
Mass (kg)	2.71576	8.70915	18.72935	13.29784	40.82998	5.24422	4.12046
Inertia (kg m^2)	0.02062	0.10596	0.32470	0.05520	2.27098	0.06020	0.04720
CG dist. (m)	0.09172	0.15815	0.17651	0.05158	0.16037	0.18767	0.07273
4	**Foot**	**Shank**	**Thigh**	**Pelvis**	**Trunk**	**UpArm**	**LwrArm**
Length (m)	0.20727	0.41324	0.40760	0.14996	0.41098	0.32931	0.26509
Mass (kg)	2.44579	7.84340	16.86753	11.97595	36.77123	4.72291	3.71086
Inertia (kg m^2)	0.02371	0.12216	0.29236	0.06733	1.55272	0.05310	0.05712
CG dist. (m)	0.10364	0.17893	0.17649	0.08259	0.13973	0.18573	0.08430
5	**Foot**	**Shank**	**Thigh**	**Pelvis**	**Trunk**	**UpArm**	**LwrArm**
Length (m)	0.17435	0.37639	0.38568	0.15333	0.44214	0.32792	0.25335
Mass (kg)	2.37045	7.60180	16.34796	11.60705	35.63855	4.57743	3.59655
Inertia (kg m^2)	0.01626	0.09822	0.25370	0.06822	1.74174	0.05104	0.05056
CG dist. (m)	0.08717	0.16298	0.16700	0.07863	0.15033	0.18495	0.08056
6	**Foot**	**Shank**	**Thigh**	**Pelvis**	**Trunk**	**UpArm**	**LwrArm**
Length (m)	0.21071	0.39583	0.44975	0.11085	0.43647	0.37080	0.26120
Mass (kg)	2.83454	9.09008	19.54856	13.87948	42.61587	5.47360	4.30068
Inertia (kg m^2)	0.02840	0.12990	0.41254	0.04264	2.02965	0.07803	0.06427
CG dist. (m)	0.10536	0.17139	0.19474	0.03927	0.14840	0.20913	0.08306

8.2 Appendix B

Least squares solution implementation in Wolfram Mathematica 9.0:

Reactions at the hand (R_{7x}, R_{7y}, T_7) are always set equal to zero and simplify out of Eqn21.

```
Eqn1 = 0 == m1 * a1x + Fgx - R1x;
Eqn2  = 0 == m1 * (a1y + g)  + Fgy - R1y;
Eqn3 = 0 == I1 * α1 - T1 - Fgy * (Cx - rx) + Fgx * Cy - R1y * (Lx - Cx) + R1x * (Ly - Cy);
Eqn4 = 0 == m2 * a2x - R2x + R1x;
Eqn5 = 0 == m2 * (g + a2y) - R2y + R1y;
Eqn6 = 0 == I2 * α2 - T2 + T1 - R1y * Cos[θ2] * (L2 - r2) + R1x * Sin[θ2] * (L2 - r2) -
     R2y * Cos[θ2] * r2 + R2x * Sin[θ2] * r2;
Eqn7 = 0 == m3 * a3x - R3x + R2x;
Eqn8 = 0 == m3 * (g + a3y ) - R3y + R2y;
Eqn9 = 0 == I3 * α3 - T3 + T2 - R2y * Cos[θ3] * (L3 - r3) + R2x * Sin[θ3] * (L3 - r3) -
     R3y * Cos[θ3] * r3 + R3x * Sin[θ3] * r3;
Eqn10 = 0 == m4 * a4x - R4x + R3x;
Eqn11 = 0 == m4 * (g + a4y ) - R4y + R3y;
Eqn12 = 0 == I4 * α4  - T4 + T3 - R3y * Cos[θ4] * (L4 - r4) + R3x * Sin[θ4] * (L4 - r4) -
     R4y * Cos[θ4] * r4 + R4x * Sin[θ4] * r4;
Eqn13 = 0 == m5 * a5x - R5x + R4x;
Eqn14 = 0 == m5 * (g + a5y )  - R5y + R4y;
Eqn15 = 0 == I5 * α5 - T5 + T4 - R4y * Cos[θ5] * (L5 - r5) + R4x * Sin[θ5] * (L5 - r5) -
     R5y * Cos[θ5] * r5 + R5x * Sin[θ5] * r5;
Eqn16 = 0 == m6 * a6x - R6x + R5x;
Eqn17 = 0 == m6 * (g + a6y )  - R6y + R5y;
Eqn18 = 0 == I6 * α6 - T6 + T5 - R5y * Cos[θ6] * (L6 - r6) + R5x * Sin[θ6] * (L6 - r6) -
     R6y * Cos[θ6] * r6 + R6x * Sin[θ6] * r6;
Eqn19 = 0 == m7 * a7x + R6x - R7x;
Eqn20 = 0 == m7 * (g + a7y ) + R6y - R7y;
Eqn21 = 0 == I7 * α7 - T7 + T6 - R6y * Cos[θ7] * (L7 - r7) + R6x * Sin[θ7] * (L7 - r7) -
     R7y * Cos[θ7] * r7 + R7x * Sin[θ7] * r7;
coefficients =
  CoefficientArrays[{Eqn1, Eqn2, Eqn3, Eqn4, Eqn5, Eqn6, Eqn7, Eqn8, Eqn9,
    Eqn10, Eqn11, Eqn12, Eqn13, Eqn14, Eqn15, Eqn16, Eqn17, Eqn18, Eqn19, Eqn20, Eqn21},
   {R1x, R1y, T1, R2x, R2y, T2, R3x, R3y, T3, R4x, R4y, T4, R5x, R5y, T5, R6x, R6y, T6}];
A = coefficients[[2]];
b = coefficients[[1]];

x = LeastSquares[A, b];
```

8.3 Appendix C: Coefficient and constant matrices

$$
\boldsymbol{A} = \begin{bmatrix}
1 & 0 & 0 & 0 & 0 & 0 \\
0 & 1 & 0 & 0 & 0 & 0 \\
Cy - Ly & Lx - Cx & 1 & 0 & 0 & 0 \\
-1 & 0 & 0 & 1 & 0 & 0 \\
0 & -1 & 0 & 0 & 1 & 0 \\
-(L2 - r2)sin(\theta 2) & (L2 - r2)cos(\theta 2) & -1 & -r2sin(\theta 2) & r2cos(\theta 2) & 1 \\
0 & 0 & 0 & -1 & 0 & 0 \\
0 & 0 & 0 & 0 & -1 & 0 \\
0 & 0 & 0 & -(L3 - r3)sin(\theta 3) & (L3 - r3)cos(\theta 3) & -1 \\
0 & 0 & 0 & 0 & 0 & 0 \\
0 & 0 & 0 & 0 & 0 & 0 \\
0 & 0 & 0 & 0 & 0 & 0 \\
0 & 0 & 0 & 0 & 0 & 0 \\
0 & 0 & 0 & 0 & 0 & 0 \\
0 & 0 & 0 & 0 & 0 & 0 \\
0 & 0 & 0 & 0 & 0 & 0 \\
0 & 0 & 0 & 0 & 0 & 0 \\
0 & 0 & 0 & 0 & 0 & 0 \\
0 & 0 & 0 & 0 & 0 & 0 \\
0 & 0 & 0 & 0 & 0 & 0
\end{bmatrix} \cdots
$$

$$
\cdots \begin{bmatrix}
0 & 0 & 0 & 0 & 0 & 0 \\
0 & 0 & 0 & 0 & 0 & 0 \\
0 & 0 & 0 & 0 & 0 & 0 \\
0 & 0 & 0 & 0 & 0 & 0 \\
0 & 0 & 0 & 0 & 0 & 0 \\
0 & 0 & 0 & 0 & 0 & 0 \\
1 & 0 & 0 & 0 & 0 & 0 \\
0 & 1 & 0 & 0 & 0 & 0 \\
-r3sin(\theta 3) & r3cos(\theta 3) & 1 & 0 & 0 & 0 \\
-1 & 0 & 0 & 1 & 0 & 0 \\
0 & -1 & 0 & 0 & 1 & 0 \\
-(L4 - r4)sin(\theta 4) & (L4 - r4)cos(\theta 4) & -1 & -r4sin(\theta 4) & r4cos(\theta 4) & 1 \\
0 & 0 & 0 & -1 & 0 & 0 \\
0 & 0 & 0 & 0 & -1 & 0 \\
0 & 0 & 0 & -(L5 - r5)sin(\theta 5) & (L5 - r5)cos(\theta 5) & -1 \\
0 & 0 & 0 & 0 & 0 & 0 \\
0 & 0 & 0 & 0 & 0 & 0 \\
0 & 0 & 0 & 0 & 0 & 0 \\
0 & 0 & 0 & 0 & 0 & 0 \\
0 & 0 & 0 & 0 & 0 & 0 \\
0 & 0 & 0 & 0 & 0 & 0
\end{bmatrix} \cdots
$$

$$
\cdots \begin{bmatrix}
0 & 0 & 0 & 0 & 0 & 0 \\
0 & 0 & 0 & 0 & 0 & 0 \\
0 & 0 & 0 & 0 & 0 & 0 \\
0 & 0 & 0 & 0 & 0 & 0 \\
0 & 0 & 0 & 0 & 0 & 0 \\
0 & 0 & 0 & 0 & 0 & 0 \\
0 & 0 & 0 & 0 & 0 & 0 \\
0 & 0 & 0 & 0 & 0 & 0 \\
0 & 0 & 0 & 0 & 0 & 0 \\
0 & 0 & 0 & 0 & 0 & 0 \\
0 & 0 & 0 & 0 & 0 & 0 \\
0 & 0 & 0 & 0 & 0 & 0 \\
1 & 0 & 0 & 0 & 0 & 0 \\
0 & 1 & 0 & 0 & 0 & 0 \\
-r5sin(\theta 5) & r5cos(\theta 5) & 1 & 0 & 0 & 0 \\
-1 & 0 & 0 & 1 & 0 & 0 \\
0 & -1 & 0 & 0 & 1 & 0 \\
-(L6 - r6)sin(\theta 6) & (L6 - r6)cos(\theta 6) & -1 & -r6sin(\theta 6) & r6cos(\theta 6) & 1 \\
0 & 0 & 0 & -1 & 0 & 0 \\
0 & 0 & 0 & 0 & -1 & 0 \\
0 & 0 & 0 & -(L7 - r7)sin(\theta 7) & (L7 - r7)cos(\theta 7) & -1
\end{bmatrix}
$$

Appendix C, cont.

$$\boldsymbol{b} = \begin{bmatrix} -a_{1x}m_1 - F_{gx} \\ -m_1(a_{1y} + g) - F_{gy} \\ F_{gy}(c_x - r_x) - c_y F_{gx} - \alpha_1 I_1 \\ -a_{2x}m_2 \\ -m_2(a_{2y} + g) \\ -\alpha_2 I_2 \\ -a_{3x}m_3 \\ -m_3(a_{3y} + g) \\ -\alpha_3 I_3 \\ -a_{4x}m_4 \\ -m_4(a_{4y} + g) \\ -\alpha_4 I_4 \\ -a_{5x}m_5 \\ -m_5(a_{5y} + g) \\ -\alpha_5 I_5 \\ -a_{6x}m_6 \\ -m_6(a_{6y} + g) \\ -\alpha_6 I_6 \\ -a_{7x}m_7 \\ -m_7(a_{7y} + g) \\ -\alpha_7 I_7 \end{bmatrix}$$

9 References

Andersen, M. S., Damsgaard, M., MacWilliams, B., & Rasmussen, J. (2010). A computationally efficient optimisation-based method for parameter identification of kinematically determinate and over-determinate biomechanical systems. *Computer Methods in Biomechanics and Biomedical Engineering*, *13*(2), 171-183.

Ashby, B. M., & Delp, S. L. (2006). Optimal control simulations reveal mechanisms by which arm movement improves standing long jump performance. *Journal of Biomechanics, 39*(9), 1726-1734.

Ashby, B. M., & Heegaard, J. H. (2002). Role of arm motion in the standing long jump. *Journal of Biomechanics, 35*(12), 1631-1637.

Bisseling, R. W., & Hof, A. L. (2006). Handling of impact forces in inverse dynamics. *Journal of Biomechanics, 39*(13), 2438-2444.

Blajer, W., Dziewiecki, K., & Mazur, Z. (2007). Multibody modeling of human body for the inverse dynamics analysis of sagittal plane movements. *Multibody System Dynamics, 18*(2), 217-232.

Bobbert, M. F., Huijing, P. A., & van Ingen Schenau, G. (1987). Drop jumping. I. the influence of jumping technique on the biomechanics of jumping. *Med Sci Sports Exerc, 19*(4), 332-338.

Busby, H. R., & Trujillo, D. M. (1987). Solution of an inverse dynamics problem using an eigenvalue reduction technique. *Computers & Structures, 25*(1), 109-117.

Busby, H., & Trujillo, D. (1997). Optimal regularization of an inverse dynamics problem. *Computers & Structures, 63*(2), 243-248.

Cahouët, V., Luc, M., & David, A. (2002). Static optimal estimation of joint accelerations for inverse dynamics problem solution. *Journal of Biomechanics, 35*(11), 1507-1513.

Chao, E. Y., & Rim, K. (1973). Application of optimization principles in determining the applied moments in human leg joints during gait. *Journal of Biomechanics, 6*(5), 497-510.

Feltner, M. E., Bishop, E. J., & Perez, C. M. (2004). Segmental and kinetic contributions in vertical jumps performed with and without an arm swing. *Research Quarterly for Exercise and Sport, 75*(3), 216-230.

Feltner, M. E., Fraschetti, D. J., & Crisp, R. J. (1999). Upper extremity augmentation of lower extremity kinetics during countermovement vertical jumps. *Journal of Sports Sciences, 17*(6), 449-466.

Filush, A. (2012). Effect of using hand-weights on performance in the standing long jump.

Hatze, H. (1981). A comprehensive model for human motion simulation and its application to the take-off phase of the long jump. *Journal of Biomechanics, 14*(3), 135-142.

Hatze, H. (2002). The fundamental problem of myoskeletal inverse dynamics and its implications. *Journal of Biomechanics, 35*(1), 109-115.

Hay, J. G. (1993). Citius, altius, longius (faster, higher, longer): The biomechanics of jumping for distance. *Journal of Biomechanics, 26*, 7-21.

Kuo, A. D. (1998). A least-squares estimation approach to improving the precision of inverse dynamics computations. *Transactions-American Society of Mechanical Engineers Journal of Biomechanical Engineering, 120*, 148-159.

Larivière, C., Gagnon, D., Gravel, D., Bertrand Arsenault, A., Dumas, J., Goyette, M., et al. (2001). A triaxial dynamometer to monitor lateral bending and axial rotation moments during static trunk extension efforts. *Clinical Biomechanics, 16*(1), 80-83.

McConville, J. T., Clauser, C. E., Churchill, T. D., Cuzzi, J., & Kaleps, I. (1980). Anthropometric relationships of body and body segment moments of inertia. *ANTHROPOLOGY RESEARCH PROJECT INC,*

Pain, M. T., & Challis, J. H. (2006). The influence of soft tissue movement on ground reaction forces, joint torques and joint reaction forces in drop landings. *Journal of Biomechanics, 39*(1), 119-124.

Payton, C., & Bartlett, R. (2007). *Biomechanical evaluation of movement in sport and exercise: The british association of sport and exercise sciences guide* Routledge.

Peters, A., Galna, B., Sangeux, M., Morris, M., & Baker, R. (2010). Quantification of soft tissue artifact in lower limb human motion analysis: A systematic review. *Gait & Posture, 31*(1), 1-8.

Plagenhoef, S., Evans, F. G., & Abdelnour, T. (1983). Anatomical data for analyzing human motion. *Research Quarterly for Exercise and Sport, 54*(2), 169-178.

Van Den Bogert, Antonie J, & Su, A. (2008). A weighted least squares method for inverse dynamic analysis. *Computer Methods in Biomechanics and Biomedical Engineering, 11*(1), 3-9.

Vanezis, A., & Lees, A. (2005). A biomechanical analysis of good and poor performers of the vertical jump. *Ergonomics, 48*(11-14), 1594-1603.

Wells, R., & Winter, D. (1980). Assessment of signal and noise in the kinematics of normal, pathological and sporting gaits. *Human Locomotion, 1*, 92-93.

Winter, D. A. (2009). *Biomechanics and motor control of human movement* Wiley. com.

Wu, W., Wu, J., Lin, H., & Wang, G. (2003). Biomechanical analysis of the standing long jump. *Biomedical Engineering: Applications, Basis and Communications, 15*(05), 186-192.